3D SIMULATION OF PHOTOELECTRON CLOUD IN KEKB LER

L. F. Wang*, H. Fukuma, K. Ohmi, S. Kurokawa, K. Oide and F. Zimmermann+
High Energy Accelerator Research Organization (KEK), Tsukuba, Ibaraki 305-0801, Japan
+CERN, Geneva, Switzerland

Abstract

A 3-dimension particle in cell simulation code is developed to study the photoelectron cloud instabilities in KEK LER. The program has been decribed in detail. Numerical examples are shown for the photoelectron motion in various kinds of magnetic fields. Simulation shows solenoid is very effective to confine the photoelectron to the vicinity of the vacuum chamber wall and make a photoelectron free region at the vacuum pipe center. The more uniform the solenoid field, the more effective the field. Multipacting can occur in drift region and dipole magnet. Special trapping occurs in quadrupole and sextupole magnets.

1 INTRODUCTION

A blow-up of the vertical beam size is observed in the KEKB positron ring (LER)[1] and it is one of the serious problems limiting the luminosity of KEKB. F. Zimmerman and K. Ohmi [2-3] explained the blow-up as a single-bunch instability of a positron bunch due to electron cloud generated by photoemission and secondary emission. The blow-up depends on the electron cloud density near the beam. Solenoid has been installed in the LER ring in order to clear the photoelectron near the beam. It was effective on reducing vertical blow-up [4]. A 3D PIC simulation code is developed to study the effects of these various magnetic field on the photoelectron formation, distribution, space charge effect, and so on. The program and some numerical examples are described in detail.

2 COMPUTER PROGRAM

The positron bunch is longitudinally divided into a number of slices according to Gaussian distribution. Such slices interact with photoelectrons transversely and oscillate according to the transfer matrix of the linear optics. Acceleration of RF cavity and synchrotron radiation are also included in longitudinal phase space.

Photoelectrons are emitted when positron slices pass through a beam pipe with length L, which is usually chosen as 1 or 2 m. A photoelectron yield of 0.1 is assumed in simulation and 30% of the photoelectrons are produced by the reflective photons. The center of photoelectron energy distribution is 5 eV with rms (root mean square) energy spread of 5 eV. In our simulation, the photoelectrons are represented by macro-particles, which move in 3-dimensional space under the force:

$$\mathbf{F}_e = \mathbf{F}_p + \mathbf{F}_{space} + \mathbf{F}_B \qquad (1)$$

where $\mathbf{F_p}$ is the force by positron beam which is given by the Bassetti Formula and $\mathbf{F_{space}}$ is the space charge force of the photoelectron. $\mathbf{F_B}$ is the force by magnetic field on the photoelectron. The result for without space charge force case has been shown in Ref. [5]. A 3D PIC space charge solver has been developed to study the space-charge force. The secondary emission is also included in the program. The simulation model is shown in figure 1.

The parameters used in the simulation are shown in table 1.

Variable	Symbol	Value
Ring circumference	C	3016.26 m
RF bucket length	s_{rf}	0.589 m
Bunch spacing	s_b	4 RF buckets
Bunch population	N	3.3×10^{10}
Average vertical betatron function	β_y	10 m
Average horizontal betatron function	β_x	10 m
Horizontal emittance	ε_x	1.8×10^{-8} m
Vertical emittance	ε_y	3.6×10^{-10} m
Betatron tune	ν_x/ν_y	45.52/44.09
Rms bunch length	σ_l	4 mm
Chamber diameter	$2R$	100 mm

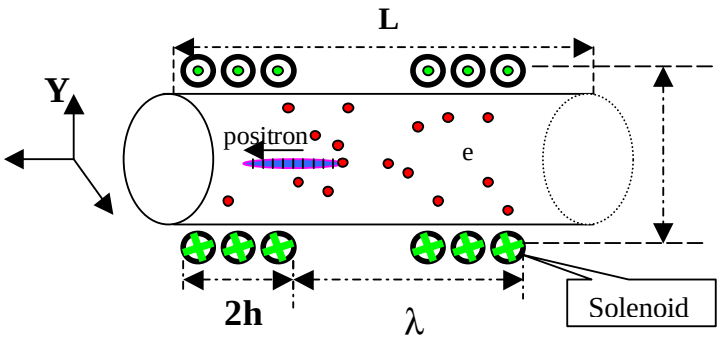

Figure 1. The scheme of the simulation model

2.1 3D PIC Space Charge Solver

The direct particle-particle method is easy for developing the program and has high accuracy.

*On leave from IHEP, Beijing

However, it has a very low efficiency. The mesh method seems to be applied by all particle simulation programs.

The vacuum chamber of LER is round shape with a radius of 50 mm. Photoelectrons are distributed within the chamber as shown in Figure 2 for solenoid case. The regular mesh as applied in the study of bunch beam case can't satisfy here because the complex shape of the vacuum chamber. Therefore, an irregular mesh is applied for the photoelectron cloud as shown in Figure 3. Similar mesh can be applied for the ante-chamber as in PEP-II.

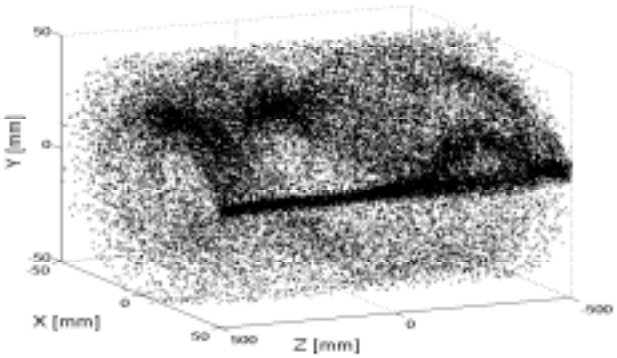

Figure 2: Example of photoelectron cloud distribution in the vacuum chamber

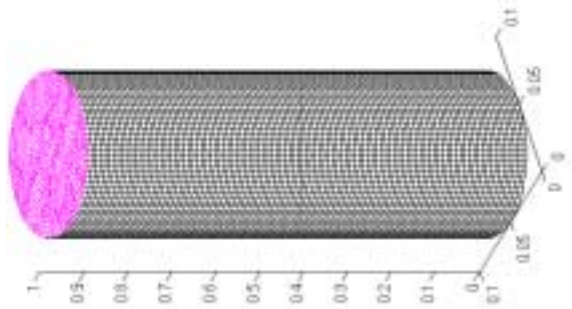

Figure 3: Mesh example of the vacuum chamber for photoelectron cloud

There are many charge assignment methods. The mesh in our method is an irregular mesh with brick elements. The charge Q_0 of a photoelectron is assigned to each node *i* of the element in which the photoelectron stays according to the shape function N_i

$$Q_i = N_i Q_0 . \tag{2}$$

Figure 4 shows the distribution of the macro-particle and charge at mesh node in one transverse section. The number of elements in this transverse section is 276, which is a small number. It already shows good representing of the real electron cloud distribution.

For the isoparametric element, the charge assignment scheme in Eq.(2) has all characters of charge assignment function such as

$$\sum_i N_i = 1 \tag{3}$$

$$\sum_i N_i \mathbf{r}_i = \mathbf{r} \tag{4}$$

The property of the shape function in Eq.(3) keeps the charge conservation. It can be called Cloud-in-a-Cell (CIC) scheme. But it is different from the so-called CIC scheme applied in general particle simulation:

(1) The general CIC method applies a regular mesh. However, our scheme uses an irregular mesh, which makes this method can be successfully applied to the complex boundary problem such as the very flat beam case and ante-chamber.

(2) General CIC is for 2D, the charge assignment function has a clear meaning such as the cloud area. There is exact the same assignment function in finite element field for the simple element, such as square element. However, Our scheme is for 3D and the assignment has not a clear physical meaning for a high order element. And, there are many kinds of elements in the finite element methods. Among them, the high order element can be applied to improve the accuracy of the method, which is much better than the nearest-grid-point assignment.

Therefore, our scheme has very serious advantages: general boundary and high accuracy. Adaptive mesh can be applied in the case of the electron concentrating at some small region, such as the long-range beam-beam simulation. However, our method is complicated to be applied comparing with the regular mesh CIC method.

The electron cloud (both the density and distribution) changes with time. We assume a quasi-static condition. The scalar potential satisfies (at each moment)

$$\Delta\phi = -\rho / \varepsilon_0 , \tag{5}$$

Eq.(5) can be solved by using the finite element method. We can get the finite element equation

$$\mathbf{A}\phi = \mathbf{B} . \tag{6}$$

Here the stiffness matrix **A** depends only on the mesh and **B** is the source term. The matrix **A** is extremely sparse and there are well-known methods for handing such linear problems, such as conjugate gradient method, profile or frontal technique. Fortunately, the vacuum chamber of LER is round shape. We can also find the Green function to get the potential. The potential ϕ at **R** is available with the Green function $G(\mathbf{R}, \mathbf{R'})$

$$\phi(\mathbf{R}) = \int_0^L dz' \int_0^{2\pi} d\theta' \int_0^a r' dr' f(\mathbf{R}') G(\mathbf{R}, \mathbf{R}') \tag{7}$$

$$G(\mathbf{R}, \mathbf{R}') = \frac{e}{L} \ln \frac{\rho^2 + r^2 r'^2 / \rho^2 - 2rr' \cos(\theta - \theta')}{r^2 + r'^2 - 2rr' \cos(\theta - \theta')}$$
$$+ \frac{4e}{L} \sum_{n=1}^{\infty} \cos nk(z - z') \left\{ K_0(nk\sqrt{r^2 + r'^2 - 2rr' \cos(\theta - \theta')}) \right.$$
$$\left. - \sum_{m=0}^{\infty} (2 - \delta_{m0}) \frac{K_m(nk\rho)}{I_m(nk\rho)} I_m(nkr) I_m(nkr') \cos m(\theta - \theta') \right\} \tag{8}$$

where L is the period length of the vacuum chamber, ρ is the pipe radius, **R'** is the source position, and **R** is the potential position, $k=2\pi/L$. The cylindrical coordinates with z-axis along the axis of the pipe, **R**=(r,θ, z), **R'**=(r',θ', z') are used.

After finding the potential, the force on each particle is interpolated by using the same shape function in order to keep the momentum conservation. Unlike the general PIC method, we calculate the force on particle directly using the potential at mesh node instead of the mesh-defined force field

$$\mathbf{E} = \sum_i \nabla N_i \cdot \phi_i \qquad (9)$$

The potential and field of the space charge at one transverse section are shown in Figure 5 for the case as Figure 4.

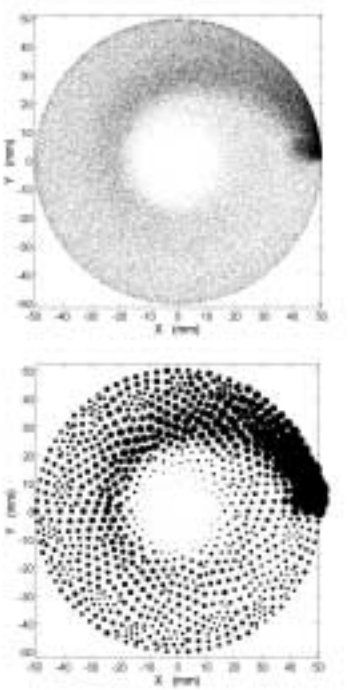

Figure 4 Charge assignment of the PIC method, Above: Transverse distribution of the macro particles in solenoid. Bottom: Transverse distribution of the mesh-defined charge by charge assignment.

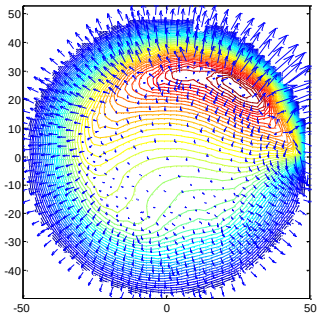

FIGURE 5 Potential and field of space charge at one transverse section

2.2 Magnetic field and beam force

Various magnetic fields can be applied and included in the program. For example, C-Yoke magnet field, solenoid, dipole magnet, quadrupole magnet and sextupole magnet. The general 3-dimensional magnetic field can be input as either formulae or tables. The following paragraphs show a few of types of the magnetic fields in KEKB.

The C-Yoke magnet can be arranged in a dipole or quadrupole configuration with equal polarity (EP) or alternating polarity (AP). For the C-yoke dipole, the field can be approximately expressed as

$$B_x = 0 \qquad (10)$$

$$B_y = a + b\cos(kz) \qquad (11)$$

$$B_z = -bk\sin(kz) \qquad (12)$$

where a=141G, b=94G, λ=0.1m and a=0, b=235G, λ= 0.2 m for the case of adjacent dipoles with equal polarity and alternating polarity, respectively. The magnet field in a C-yoke quadrupole is

$$B_x = (a + b\cos kz)y \qquad (13)$$

$$B_y = (a + b\cos kz)x \qquad (14)$$

$$B_z = -bk\sin(kz)xy \qquad (15)$$

where a=0.3T/m, b=0.2T/m, λ=0.1m and a=0, b=0.5T/m, λ=0.2m for the equal polarity and alternating polarity, respectively.

When the periodic solenoids are arranged with the same current direction in the coil, we call this kind of arrangement equal polarity configuration. In this case, the magnetic field can be approximately expressed as

$$B_z(x,y,z) = B_{z0} + B_0\sin kz\,, \qquad (16)$$

$$B_x(x,y,z) = -0.5B_0 kx\cos kz\,, \qquad (17)$$

$$B_y(x,y,z) = -0.5B_0 ky\cos kz\,. \qquad (18)$$

When the solenoids current takes alternating direction, which is called alternating polarity configuration, the longitudinal filed is expressed as

$$B_z(x,y,z) = B_0\sin kz \qquad (19)$$

The transverse field components are the same as equal polarity case.

Most of bending magnets in LER are normal bending magnets with B=0.848T. Typical quadrupole and sextupole field gradient are 10.3 T/m and 350 T/m^2 KEKB LER, respectively.

The positron bunch is assumed rigid gaussian distribution. The kick on photoelectrons is given by the Bassetti formula

$$\Delta\upsilon_y + i\Delta\upsilon_x = Nr_e c\cdot\sqrt{\frac{2\pi}{\sigma_{x,y}(\sigma_x+\sigma_y)}}\,f(x,y)\,,$$

$$f(x,y) = w\left(\frac{x+iy}{\sqrt{2(\sigma_x^2-\sigma_y^2)}}\right) -$$

$$\exp(-\frac{x^2}{2\sigma_x^2}-\frac{y^2}{2\sigma_y^2})w\left(\frac{x\sigma_y/\sigma_x+iy\sigma_x/\sigma_y}{\sqrt{2(\sigma_x^2-\sigma_y^2)}}\right) \quad (20).$$

where σ_x and σ_y are the positron bunch transverse size.

The image current effect is also included in the program. The shape of the vacuum chamber in KEKB LER is round. Therefore, the image current is easily found. In case of the arbitrary chamber shape, PIC method can be applied for the space charge force of the positron bunch.

3 SIMULATION EXAMPLES

The build up and the distribution of electron cloud (e-cloud) in a few of typical magnetic fields are discussed in this section.

3.1 Effect of C-Yoke magnet and solenoid field on the confinement of the photoelectrons

Permanent C-yoke magnets were attached to vacuum ducts to sweep out the electrons from November 1999 to July 2000. The photoelectron cloud density near the beam is non-zero for all C-yoke magnet configuration as shown in figure 6 for equal polarity quadrupole configuration. However, it is zero for equal polarity solenoid with B_{z0}=30 Gauss, B_0=20 Gauss and $\lambda=2\pi/k$=1 m as shown in figure 4. Simulation studies show that uniform longitudinal solenoid field is better. Details about the solenoid effect on the photoelectron cloud can be found from reference [6]. The conclusion is that solenoid is better than C-yoke magnet. The solenoid effect also has been studied in reference [7]. The photoelectron cloud density near the beam is non-zero in reference [7], which is different from our result.

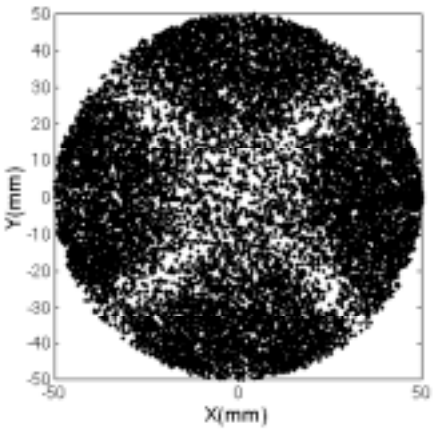

Figure 6 Electron cloud distribution in C-Yoke quadrupole with equal polarity configuration

Figure 7 shows the photoelectron distribution on the chamber wall in the solenoid field case. The photoelectrons hit the chamber wall and lost or produce secondary electrons. The solenoid field is non-uniform in longitudinal direction, which causes the lost cloud distribution also longitudinal position dependent. The azimuth angle distribution of the lost photoelectron depends on the current direction in the solenoid coil because different longitudinal magnetic field direction will cause different deflexion direction of the photoelectron motion. As a result, the current of photoelectron monitor depends on both the longitudinal position of the monitor and the current direction in solenoid coil.

The photoelectrons in solenoid field couldn't receive more energy from the positron bunch because they are confined far from the chamber center by solenoid magnetic field. Therefore, there is no multi-pacting in solenoid case. The heat-load on the chamber wall due to the hitting of the photoelectrons is also smaller for the same reason. It can be concluded that solenoid works very well with zero photoelectron density at chamber center and lower heat-load on the chamber wall because there is no multi-pacting in this case.

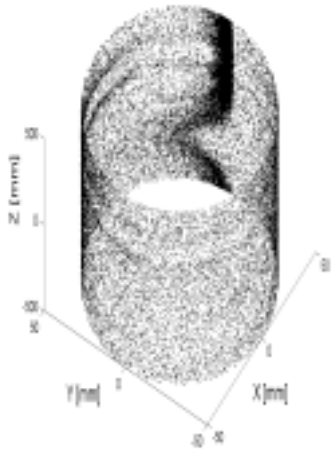

Figure 7 Lost Cloud Distribution around the chamber wall in solenoid case.

3.2 Multi-pacting in drift region and dipole magnet

In drift region, the photoelectrons are focused by the force of the positron bunches and then there is a very larger photoelectron density at chamber center. The photoelectrons near the chamber center cloud receive more energy from the positron bunches. Such higher energy photoelectrons then cause multi-pacing when they hit the chamber wall. The photoelectron density at the chamber center is $10^{13}m^{-3}$, which is 10 times larger than the saturation level. The transverse distribution of the photoelectron cloud in drift region is shown in figure 8. Heat-load is also a serious problem in drift region because photoelectron can receive more energy from positron bunches and the amount of lost photoelectrons on the wall is large. Drift region is the most dangerous case on both beam dynamics and heat-load.

Figure 9 shows the photoelectron cloud distribution inside dipole magnet. Two multi-pacting regions are clear shown in the figure. The central region is non-

multipacting region because the photoelectrons moves along the vertical field lines with the horizontal coordinate around zero cloud receive more energy. The energy of the photoelectrons decreases from horizontal center to both sides. On the other word, the energy of the photoelectrons decreases with the horizontal coordinate |x| as the shown in figure 10. As we known, the true secondary emission yield is smaller than one for photoelectrons with both very large and small energy. As a result, multi-pacting happens in the two regions near the chamber center. The position of the multi-pacting region depends on the energy of the photoelectrons, which is decided by the interaction of photoelectrons and positron bunches. Therefore, the filling patter of the beam, such as bunch current and bunch spacing, can change the multi-pacting area. In general, when the bunch current increase, the multi-pacting region will move to the area with larger |x| and the width of multi-pacting region also will increase at the same time. The exact results depend on the interaction between the photoelectron cloud and positron bunches. The mechanism of the multi-pacting in dipole magnet is clearly shown in figure 10.

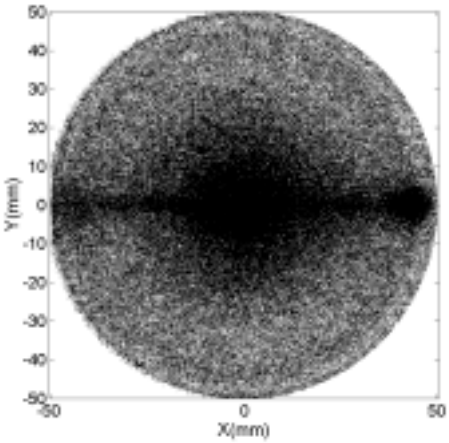

Figure 8 Electron cloud distribution in drift region

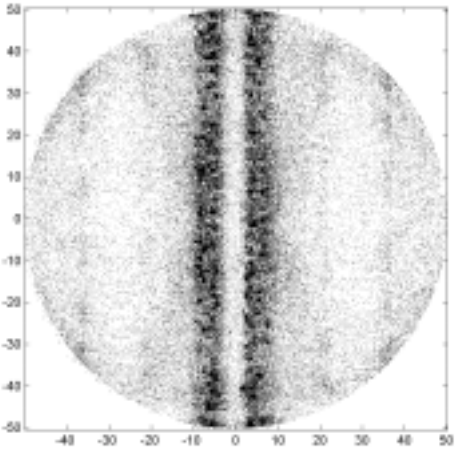

Figure 9 Electron cloud distribution in dipole magnet

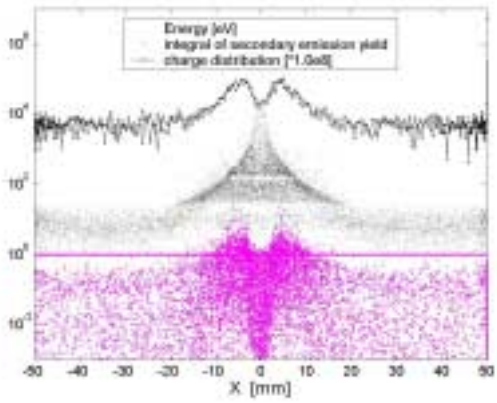

Figure 10 Mechanism of the multi-pacting in dipole magnet. Black dot is the energy of photoelectrons which hit the chamber wall. Pink dot shows the multiply of secondary emission yield of the photoelectrons which hit the wall. The black solid shows the lost photoelectron charge distribution.

3.3 Photoelectron Trapping in quadrupole and sextupole magnets

It is very interesting that more than 90% of the photoelectrons can be seriously trapped by quadrupole and sextupole magnetic field during the bunch train separation as shown in figure 11. The photoelectron density is almost constant during the train gap in these two fields. However, the density decays quickly in dipole magnet. Figure 12 shows one typical trapped electron orbit in normal quadrupole field during the train gap. The drift time is about 960ns. The trapped electron spirals in an ever-tighter orbit along the magnetic field line when the field becomes stronger, converting more and more translational energy into energy of rotation until its velocity along the field line vanish. Then the electron turns around, still spiraling in the same sense, and move back along the field line. Figure 13 shows the electron-trapping phenomena in normal sextupole. The electron-trapping phenomena are very similar with the plasma trapping in the mirror magnetic field.

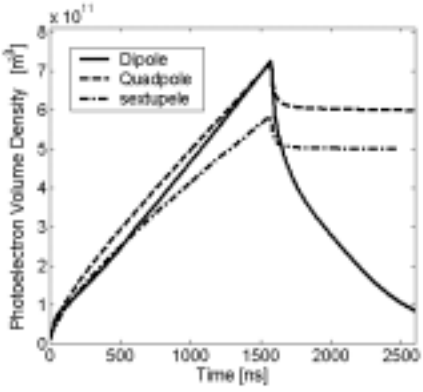

FIGURE. 11 Photoelectron average volume density in different magnet fields as a function of time for a train

with 200 bunches spaced by 7.86 ns and followed by a long gap.

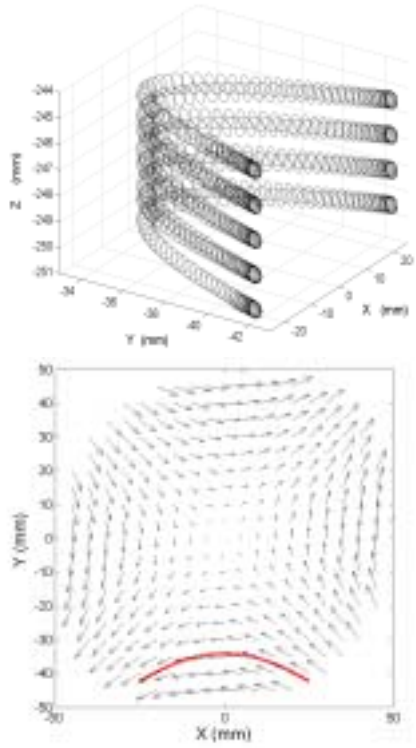

Figure 12 Photoelectron Trapping in Quadrupole Magnetic Field During the Train Gap. Above: 3D orbit; Bottom: 2D orbit (red line) and quadrupole field (black arrow)

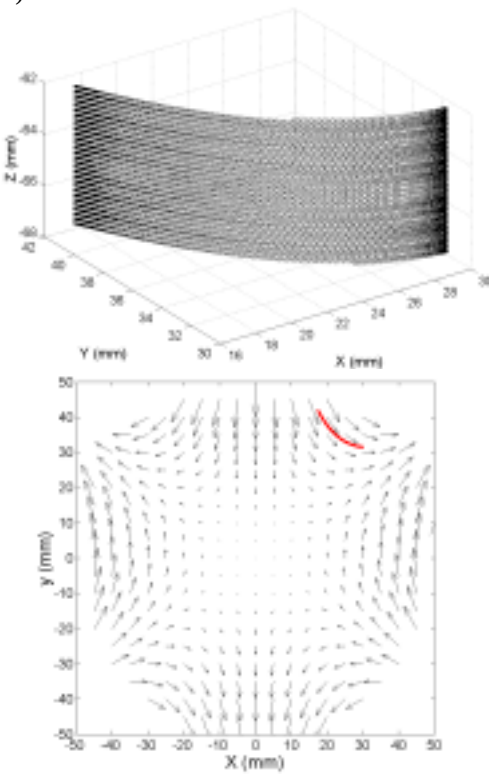

Figure 13 Photoelectron Trapping in Normal Sextupole Magnetic Field During the Train Gap. Above: 3D orbit; Bottom: 2D orbit (red line) and sextupole field (black arrow).

We first describe the motion of photoelectron in pure magnetic field and then focus on the effects of positron beam.

First we consider the case of no electric field, which is almost true for electron cloud during the bunch train-separation where the space charge potential of the electron cloud is neglectable comparing with the magnetic potential in normal magnets. Since the direction of magnetic force acting on the electron is perpendicular to the electron velocity, the electron kinetic energy is therefore conserved,

$$W = \frac{m\upsilon^2}{2} = cons\tan t \tag{21}$$

The motion of the electron in magnetic field can be regarded as the superposition of the gyration motion around the guiding center and the motion of the guiding center. The gyration motion of electron is a rapid rotation around the magnetic field line. The motion of the guiding center is the average motion over the gyration.

Consider the case in which the magnetic field slowly varies in space. The variation is assumed to be sufficiently slow that the magnetic field at the electron position hardly changes during the cyclotron motion. This is true for our case where the magnetic filed is strong except for the central region of the chamber and the electron energy is low, which means small Larmor radius and short period. While the period of a spiraling electron changes as it moves into regions where the magnetic field is weaker or stronger, the product $T \times E$, the period T times the energy E, is almost a constant. It is not an exact constant, but if the rate of change is slow enough, e.g. if the field changes rather slowly, it comes very close. A certain quality, an "adiabatic invariant", is almost kept at a constant value. In more general way, the action of a system with canonical variables *q* and *p*, defined by

$$J = \oint pdq \tag{22}$$

is a constant under a slow change in an external parameter. Here " represents an integral over one period of the motion. Therefore, for such a quasi-periodic motion, there exists two adiabatic invariation given by [8]

$$J_\perp = \oint m\upsilon_\perp \rho_s d\varphi = \frac{4\pi m}{e}\mu_m, \tag{23}$$

$$J_\parallel = \oint m\upsilon_\parallel dl, \tag{24}$$

where

$$\mu_m = \frac{m\upsilon_\perp^2}{2B} \tag{25}$$

is the magnetic moment, $\upsilon_\perp$ is the gyration velocity, $\rho_s = \frac{m\upsilon_\perp}{|e|B}$ is the Larmor radius and υ is the parallel or longitudinal velocity which is parallel to the magnetic field. $J_\perp$ and J are called the transverse and parallel adiabatic invariation, respectively.

As the guiding center of the electron moves along the field line, which will be explained below, the magnetic field strength at the electron changes. Because the magnetic moment and kinetic energy of the electron are conserved, the kinetic energy of the parallel motion varies according to the relation

$$\frac{1}{2}m\upsilon_\parallel^2 + \mu_m B = const. \qquad (26)$$

Recalling the motion of a pendulum in the earth weight potential, Eq.(26) implies that the guiding center motion along the field line behaves like a particle motion in a magnetic potential energy $\mu_m B$. The magnetic field is mirror field in quadrupole and sextupole magnets, in which magnetic filed is weaker at the center and is stronger at both ends of the mirror field line. When the guiding center of electron moves along the field line from weaker field region to stronger field region, the parallel velocity decreases and the gyration velocity increases and the electron is heated. This kind of heating is called adiabatic heating in the plasma field. Therefore, the electron spirals in an ever-tighter orbit because the period of gyration motion and parallel velocity become smaller and smaller. When the electron comes to the point where the parallel velocity vanishes, the electron direction of motion is reversed. The parallel velocity of the reflected electron is increased when it moves along the field line and gets maximum value at the weakest field point (mirror point). Then it continues a similar motion along the other side of the mirror point. Such kind of trap is called magnetic mirror trap. The motion of electron in mirror field is shown in figure 14. The trap condition is

$$m\upsilon_\parallel^2 / 2 < \mu_m (B_{\max} - B), \qquad (27)$$

where υ is the parallel velocity at position with magnetic field B, B_{max} is the maximum magnetic field along this field line, which is located near the vacuum chamber wall in our case. Note the trap strongly depends on the electron velocity υ_0 and $\upsilon_{\perp 0}$. According to Eqs. (21), (23) and (25), the trap happens if

$$\frac{\upsilon_{\perp 0}^2}{\upsilon_{\perp 0}^2 + \upsilon_{\parallel 0}^2} > \frac{B_0}{B_{\max}}, \qquad (28)$$

where B_0 is the field at one position with velocity υ_0 and $\upsilon_{\perp 0}$. The trap condition Eq.(28) can be more conveniently described as

$$\Gamma_{trap} > 1 \qquad (29)$$

with the trap factor

$$\Gamma_{trap} = \frac{F_\upsilon}{F_B} = \frac{\upsilon_{\perp 0}^2}{\upsilon_{\perp 0}^2 + \upsilon_{\parallel 0}^2} \frac{B_{\max}}{B_0}. \qquad (30)$$

Where F_υ and F_B is left and right part of Eq. (28), respectively. When the trap factor Γ_{trap} is bigger than 1, the electron is trapped.

According Eqs. (29-30), a photoelectron could be trapped if its kinetic energy of gyration motion increases. The electron can receive transverse energy around the mirror point where the electric field direction of positron bunch is in the gyration motion plane. However, a short bunch is required for the electron to efficiently receive transverse energy because the effect of a long positron bunch on the transverse energy can cancel over many periods of gyration motion. Therefore, a short positron bunch, when compared with the cyclotron period at the mirror point, is very effective to increase the photoelectron energy distribution F_υ by increasing the kinetic energy of the gyration motion and then can cause the trapping of the photoelectrons. In the case of short positron bunch, electrons can get more kinetic energy of the gyration motion around the mirror points due to the high beam potential at that point and the short interaction time. A long positron bunch has less average effect on transverse energy of the photoelectron for all the field lines. Therefore, there the effect is weak on the trap of the photoelectron. The trapping requirement for positron bunch length can be described as

$$\sigma_l < \frac{2\pi cm}{e}\frac{1}{B} \qquad (31)$$

where B is the field at the mirror point. Eq.(31) can be written in a more convenient way as $\sigma_l(mm) < 10.7/B(T)$, which means the positron bunch length should be shorter than 10.7 mm for a field line with 1 T magnetic field at the mirror point.

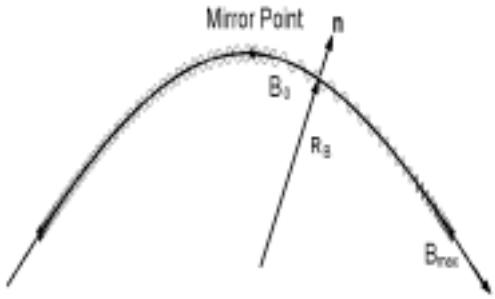

Figure 14 Motion of electron in a mirror magnetic field

3.4 Heat-load of photoelectron cloud

The lost photoelectrons, which hit the chamber wall, can cause the temperature increment of the vacuum chamber. The heat-load depends on the quantity and energy of the photoelectrons which hit the vacuum chamber wall. In drift region, the photoelectrons have

higher energy and larger quantity due to the multi-pacting. Therefore, there are larger loss rate of photoelectrons on the wall and higher heat-load. Multi-pacting occurs in two small regions in dipole magnet. The heat-load distribution is also two peaks at these two multi-pacting regions. On the other hand, there is lower heat-load in solenoid and quadrupole and sextupole cases where multi-pacting couldn't occur. Figures 15-16 show the lost photoelectron charge and heat-load azimuth angle distribution for the different fields.

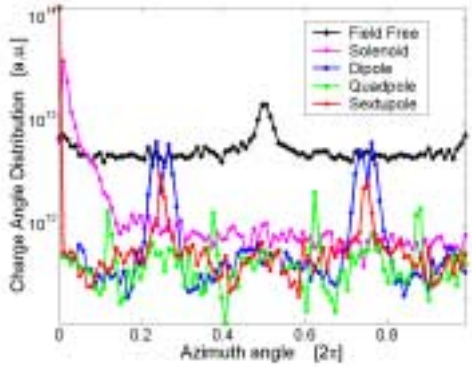

Figure 15 Charge azimuth angle distributions of the lost photoelectrons in different fields, which hit the vacuum chamber wall.

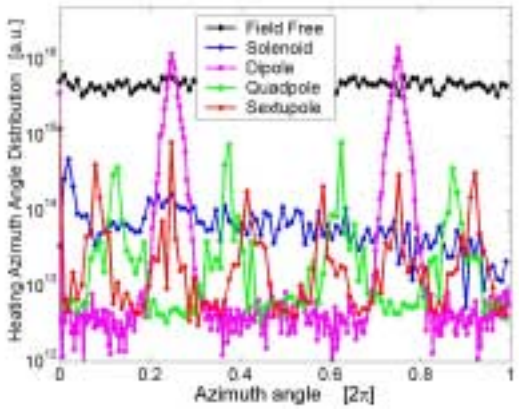

Figure 16 Heat-load azimuth angle distributions due to the lost photoelectrons in different fields, which hit the vacuum chamber wall.

3.5 Build up of electron cloud

Figures 17-18 show the average and center volume density in different magnetic fields as a function of time for a train with 200 bunches spaced by 7.86 ns and followed by a long bunch train gap. The saturation time decay time during the bunch train gap in field free case is the shortest because there is no magnetic field to confine the photoelectrons. One the other hand, the decay time is very large in quadrupole and sextupole magnet due to the deep trapping. The preliminary photoelectrons don't contribute to the make-up of the photoelectron cloud in dipole, quadrupole and sextupole magnets. At the same time there is a trapping phenomenon in quadrupole and sextupole magnets and there is muti-pacting phenomenon in dipole magnet. All these characters cause the average cloud density in these three fields is almost a linear function of the time during the build-up process.

The photoelectron density near the beam is zero in solenoid case and is small in quadrupole and sextupole cases. Therefore, the deeply trapped photoelectrons in quadrupole and sextupole magnets mainly contribute to the coupled bunch instabilities. The photoelectron densities near the beam in drift region and dipole is bigger. Photoelectron in these two cases is important for the blow-up of the positron bunch.

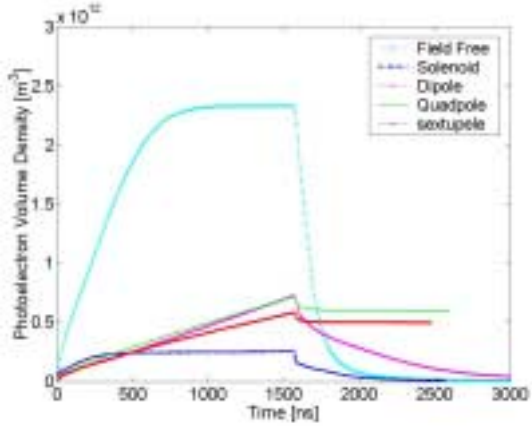

Figure 17 Photoelectron average volume densities in different magnet field as a function of time for a train with 200 bunches spaced by 7.86 ns and followed by a long bunch train gap.

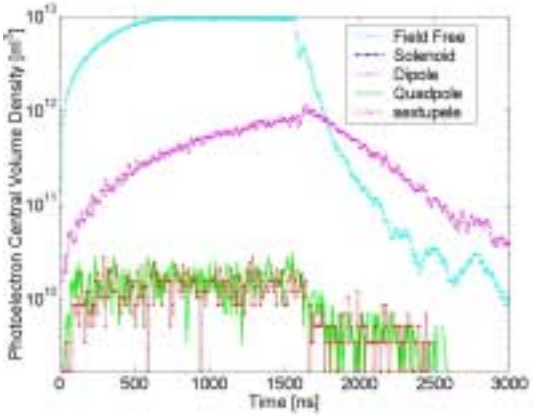

Figure 18 Photoelectron volume densities at pipe center for different magnet field cases as a function of time for a train with 100 bunches spaced by 7.86 ns and followed by a long bunch train gap.

4 SUMMARY AND CONCLUSIONS

A complete 3D PIC program has been developed. The Particle-In-Cell (PIC) method is applied to the 3D space charge of the photoelectron cloud. The simulation shows that the magnetic field can reduce the electron density at the pipe center. Uniform solenoid field is the most effective field to confine the

photoelectron to the vicinity of the vacuum chamber wall and solenoid is better than other kind of magnets. Solenoid works well with zero photoelectron central density and lower heat-load. Multi-pacting occurs in drift region and dipole magnet. A serious electron-trapping phenomenon during the train gap has been found in normal quadrupole and sextupole, whose mechanism is the mirror magnetic field trap.

5 ACKNOWLEDGEMENT

We thank Prof. A. Chao, K. Nakajima and E. Perevedentsev for helpful discussion. Thank KEKB commissioning group for all their help, information and discussion.

6 REFERENCE

[1] H. Fukuma, et al., “Observation of vertical beam blow-up in KEKB low energy ring”, EPAC2000, 2000.

[2] F.Zimmermann, "Electron-Cloud Studies for the Low-Energy Ring of KEKB", CERN-SL-Note-004, 2000.

[3] K. Ohmi and F. Zimmermann, “Head-tail instability caused by electron cloud in positron storage rings”, Physics Review Letter (85): 3821, 2000.

[4] H. Fukuma et al., "Study of vertical beam blowup in KEKB low energy ring", HEACC2001.

[5] L. Wang, et al., "3D simulation of photoelectron cloud ", 2001 Particle Accelerator Conference (PAC2001) CHICAGO, ILLINOIS USA, JUNE 18-22, 2001.

[6] L.F. Wang, H. Fukuma, K. Ohmi, "Simulation Study of Photoelectron Motion in Solenoid Field", KEK-2001-2, 2001.

[7] F.Zimmermann,“Electron Cloud at the KEKB Low Energy Ring:Simulations of Central Cloud Density, Bunch Filling Patterns,Magnetic Fields,and Lost Electrons ”,CERN-SL-2000-017 (AP)(May,2000).

[8] Kenro Miyamoto, Plasma Physics for Nuclear Fusion. (MIT Press, Cambridge, Massachusetts, and London, England, 1980).